A theoretical framework for multi-species range expansion in spatially heterogeneous landscapes

Eigentler, Lukas; Stanley-Wall, Nicola R.; Davidson, Fordyce A.

Published in:
Oikos

DOI:
10.1111/oik.09077

Publication date:
2022

OIKOS

Research

A theoretical framework for multi-species range expansion in spatially heterogeneous landscapes

Lukas Eigentler, Nicola R. Stanley-Wall and Fordyce A. Davidson

L. Eigentler (https://orcid.org/0000-0002-8333-8132) ✉ (leigentler001@dundee.ac.uk) and N. R. Stanley-Wall (https://orcid.org/0000-0002-5936-9721), Division of Molecular Microbiology, School of Life Sciences, Univ. of Dundee, Dundee, UK. – LE and F. A. Davidson (https://orcid.org/0000-0002-8377-3863), Mathematics, School of Science and Engineering, Univ. of Dundee, Dundee, UK.

Oikos
2022: e09077
doi: 10.1111/oik.09077
Subject Editor: Justin Travis
Editor-in-Chief: Dries Bonte
Accepted 31 March 2022

Range expansion is the spatial spread of a population into previously unoccupied regions. Understanding range expansion is important for the study and successful management of ecosystems, with applications ranging from controlling bacterial biofilm formation in industrial and medical environments to large scale conservation programmes for species undergoing climate-change induced habitat disruption. During range expansion, species typically encounter competitors. Moreover, the spatial environment into which expansion takes place is almost always heterogeneous. Nevertheless, the impact of competition and spatial landscape heterogeneities on range expansion remains understudied. In this paper we present a theoretical framework comprising two competing generic species undergoing range expansion and use it to investigate the impact of spatial landscape heterogeneities on range expansion with a particular focus on its effect on competition dynamics. We reveal that the area covered by range expansion is highly variable due to the landscape heterogeneities. Moreover, we report significant variability in competitive outcome (relative abundance of a focal species), but determine that this is induced by low initial population densities and is independent of landscape heterogeneities. We further show that both area covered by range expansion and competitive outcome can be accurately predicted by a Voronoi tessellation with respect to an appropriate metric, which only requires information on the spatial landscape and the response of each species to that landscape. Finally, we reveal that if species interact antagonistically during range expansion, the dominant mode of competition depends on the initial population density; antagonistic actions determine competitive outcome if the initial population density is high, but competition for space is the dominant mode of competition if the initial population density is low. These findings enhance our understanding of how competition for space and antagonistic interactions affect range expansion in spatially heterogeneous environments and provide a predictive tool for future species-specific approaches.

Keywords: coexistence, competition, Lotka–Volterra, range expansion, spatial heterogeneity

NORDIC SOCIETY OIKOS

www.oikosjournal.org

Introduction

The spread of a population into space previously unoccupied by that population is commonly referred to as range expansion. This is a ubiquitous phenomenon. For example, range expansion occurs during growth of microbial colonies (Hallatschek et al. 2007, Buttery et al. 2012), ecological invasions (Okubo et al. 1989, Hastings et al. 2005, Pejchar and Mooney 2009, Fraser et al. 2015), the spread of epidemics (Diekmann 1979, Artois et al. 2018) and even human migration (Templeton 2002, Moreau et al. 2011). Notably, range expansion is not just a feature of the early history of a species (e.g. spread of a new disease), but also occurs due to changes to the environment such as those induced by climate change (with habitats typically shifting towards poles or higher elevations) (Hill et al. 2001, Rosenzweig et al. 2007, Vos et al. 2008, Wilson et al. 2009). Under current policies, climate change is predicted to accelerate species extinction and, as of 2015, is estimated to be threatening over 15% of species globally (Urban 2015). Therefore, better understanding how range expansion enables species to track shifts of habitable environments is becoming increasingly important (Rosenzweig et al. 2007). Knowledge of the fundamental dynamics that govern range expansion will provide insights into the resilience of species to climate change (MacDonald and Lutscher 2018) and could provide opportunities for landscape management as part of conservation programmes (Vos et al. 2008, Wilson et al. 2009). As range expansion typically takes place over large spatial scales (compared to the size of an individual), populations are likely to encounter spatially heterogeneous landscapes (With 1997, Hill et al. 2001, With 2002, Fraser et al. 2015, Crone et al. 2019).

Most ecological systems are underpinned by competitive dynamics between species (Levine and HilleRisLambers 2010, Valladares 2015). Therefore, during range expansion, populations typically comprise different species that compete for space and resources by means of spatial expansion and other competitive interactions. Previous studies have addressed many different facets involved in multi-species range expansion; for example, interspecific competition has been shown to slow the speed of range expansion and also affect the shape of the population fronts (Legault et al. 2020); successive range expansion of different species has been shown to enable coexistence with a fractal-like structure in the population (Goldschmidt et al. 2017); classical results on non-transitive competitive hierarchies have been highlighted to not necessarily apply to multi-species range expansion (Weber et al. 2014); and genetic drift at population fronts during range expansion has been shown to lead to a loss of genetic diversity (Hallatschek et al. 2007). While the impact of spatial heterogeneity in the landscape on both the evolutionary dynamics in range expansion (Wegmann et al. 2006, Gralka and Hallatschek 2019) and single-species expansion fronts (Kinezaki et al. 2010, Hodgson et al. 2012, Möbius et al. 2021) has previously been investigated, its impact on competition for space and its interplay with other interspecific competition dynamics during range expansion remain understudied.

From a theoretical perspective, competition dynamics in biological and ecological systems are most commonly characterised by their asymptotic behaviour – often an equilibrium state (Chesson 2000, McPeek 2012). However, such an approach is not suitable for description of range expansion as this asymptotic procedure fails to account for the importance of the invasion dynamics (Travis and Dytham 2002, Ghosh et al. 2015). Instead, non-equilibrium analyses of range expansion have been employed that are restricted to a finite time interval with results typically reported from a fixed, predefined endpoint (Hallatschek et al. 2007, Weber et al. 2014, Goldschmidt et al. 2017, Legault et al. 2020). The importance of space to competition dynamics in equilibrium settings is a well-explored topic. Spatially-extended dynamics are known to enable species coexistence at equilibrium in some cases in which competition in well-mixed conditions would lead to competitive exclusion. One classical example is a tradeoff between dispersal abilities and local competitiveness (Levins and Culver 1971, Horn and MacArthur 1972). Such a tradeoff creates behavioural niches (Whittaker et al. 1973), which enable a locally weaker species to persist in a population if it is able to colonise new areas more rapidly than its locally superior competitor(s) (Tilman 1994). Thus, a tradeoff between local competitiveness and colonisation abilities creates a balance that enables coexistence through spatial segregation (Levins and Culver 1971, Horn and MacArthur 1972, Hassell et al. 1994, Tilman 1994, Gravel et al. 2010). Similarly, coexistence in a spatially segregated equilibrium state can also be induced by non-transitive competitive hierarchies of three or more species, usually referred to as 'rock–paper–scissor dynamics' (Kerr et al. 2002, Reichenbach et al. 2007, Avelino et al. 2019, Lowery and Ursell 2019).

Many antagonistic competitive interactions that take place in a spatially extended context require, at a fundamental level, spatial co-location. Hence, competition for space and competition through antagonistic actions are intrinsically linked. To understand the precise dynamics of competitive mechanisms affecting range expansion, it is therefore key to first attain knowledge about the role of spatial dynamics, in particular those that lead to spatial segregation. In a previous paper, we investigated the role of competition for space between two biofilm-forming bacterial strains in the specific case of microbial range expansion on spatially homogeneous substrates (Eigentler et al. 2022). In brief, we revealed that in a homogeneous spatial landscape, the initial population density has a significant impact on competitive outcome (defined to be the relative abundance of one focal species across the whole community). Starting with a fixed 1:1 ratio between populations in a spatially homogeneous landscape, high initial densities consistently led to an equal competitive outcome. By contrast, random seeding of the initial population at low densities resulted in highly variable competitive outcomes. Furthermore, in Eigentler et al. (2022), we defined a predictive tool that could be used to determine competitive outcome based solely on the distribution of the initial population. In short, the method is as follows. A circle was first drawn around the initial population. Next, for each point on the circle, the closest initial population patch was determined

and the point on the circle labelled correspondingly. Finally, this labelling was used to define an index, termed the 'access to free space score', that quantified the proportion of points on the circle associated with each strain (Fig. 1). For fixed initial population density, we revealed a remarkably strong linear correlation between the access to free space score and the competitive outcome of a strain.

In this study, we focus on the interplay of competition for space and antagonistic interactions in multi-species range expansion that takes place in spatially heterogeneous landscapes. We first confirm that, all else being equal, changes in a spatially heterogeneous landscape across different realisations of range expansion represent an additional source of variability. Based on this observation, we investigate 1) whether the the random seeding of the initial population remains the determinant of variability in competitive outcome or whether changes in the spatial landscape become dominant; 2) if predictions of spatial spread and competitive outcome during range range expansion can be made based on the initial population distribution despite the heterogeneities in the landscape; and 3) whether competition for space or antagonistic interactions are the dominant competitive mode during range expansion or whether there is a fundamental dependence on the spatially heterogeneous landscape.

We first present the mathematical framework and methods used in the model analysis in section 'Theoretical framework'. The results of our model analysis are presented next in section 'Results: Range expansion in 273 spatially heterogeneous domains', where we first focus on competition for space (section 'Competition for space'). Then, we investigate the impact of the interplay of spatial dynamics and antagonistic mechanisms (section 'Antagonistic interactions'). Finally, we discuss the implications of our results.

Theoretical framework

Model

Multi-species range expansion can be abstracted to the interplay between the key processes of (net) local growth, dispersal and interspecific interactions. We capture these dynamics in a mathematical framework and account for spatial heterogeneity in the landscape by employing space-dependent dispersal coefficients and growth rates. These heterogeneities represent variations in environmental conditions, such as the availability of growth limiting nutrients.

The model describes the dynamics of two generic species $B_1(\mathbf{x},t)$ and $B_2(\mathbf{x},t)$ and tracks their dynamics using as system of partial differential equations (PDEs) based on the spatially extended competitive Lotka–Volterra equations:

$$\frac{\partial B_1}{\partial t} = \nabla \cdot \left(d_1(\mathbf{x}) \left(1 - \frac{B_1 + B_2}{k} \right) \nabla B_1 \right) + r_1(\mathbf{x}) B_1 \left(1 - \frac{B_1 + B_2}{k} \right) - c_{12} B_1 B_2 \quad , \tag{1a}$$

$$\frac{\partial B_2}{\partial t} = \nabla \cdot \left(d_2(\mathbf{x}) \left(1 - \frac{B_1 + B_2}{k} \right) \nabla B_2 \right) + r_2(\mathbf{x}) B_2 \left(1 - \frac{B_1 + B_2}{k} \right) - c_{21} B_1 B_2 \quad . \tag{1b}$$

Here $\mathbf{x} \in \Omega$ is a point in a two-dimensional circular spatial domain $\Omega = \{\mathbf{x} \in \mathbb{R}^2 : \| \mathbf{x} \| < R_\Omega\}$ for some positive constant R_Ω (arbitrary space units) and time $t \geq 0$ (arbitrary time units). To preserve generality, we choose a simple, logistic law as a representative form of local population growth, where $r_1(\mathbf{x}) \geq 0$ and $r_2(\mathbf{x}) \geq 0$ denote the maximum growth rates of B_1 and B_2, respectively, and $k > 0$ the carrying capacity. Note that growth is limited by the total population density and again for simplicity we assume the carrying capacity to be constant. This represents growth limitation due to intraspecific and interspecific competition for resources, such as nutrients or space. Dispersal is assumed to be random and is modelled by a diffusion term. However, diffusion of either species into occupied territories is assumed to be limited by the resident population. This limitation in dispersal is a common feature of interacting systems across a range of scales. Examples include interacting microbial populations (Stefanic et al. 2015,

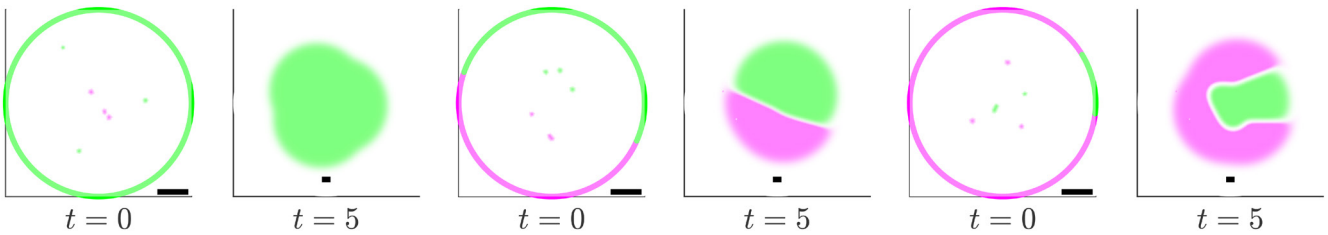

Figure 1. Predictions of competitive outcome in a spatially homogeneous landscape. Three example realisations of Eq. 2.1 on a spatially homogeneous landscape with $N=6$ initial population patches are shown. The parameter values are $r_1 = r_2 = 5$, $d_1 = d_2 = 0.1$, $c_{21} = 10$ and $c_{12} = 50$. Note that these parameter values mean that both species are governed by the same growth dynamics in the absence of a competitor, but that B_2 (green) is the intrinsically stronger species under competition (B_1 is shown in magenta). The initial condition is classified by drawing a circle around the initial population and determining the closest initial patch to each point on the circle. Note that the visualisation of the initial condition shows a blow-up of the domain centre only. The scale bar is one unit length in all figures. This figure is adapted from (Eigentler et al. 2022) in accordance to its CC-BY 4.0 International license.

Matoz-Fernandez et al. 2020) and territorial animal species (Cozzi et al. 2018). Limitation is accounted for in the model through density-dependent flux terms that decrease with total population density from their respective maxima $d_1(\mathbf{x}) \geq 0$ and $d_2(\mathbf{x}) \geq 0$ at $B_1 + B_2 = 0$ to zero at $B_1 + B_2 = k$ (Korolev et al. 2012) (see the discussion and Supporting information for a comparison with standard diffusion). Moreover, upon contact, species are assumed to engage in antagonistic actions leading to additional death or growth reduction between both species not accounted for by the logistic growth terms. The constants $c_{12} \geq 0$ and $c_{21} \geq 0$ denote the respective antagonistic rates. For brevity, we refer to these antagonistic interactions as 'killing terms'. However, we note that that these interaction terms could be assimilated into the standard form of the Lotka–Volterra equations with intraspecific competition coefficients $r_1(\mathbf{x})/k$ and $r_2(\mathbf{x})/k$ and interspecific competition coefficients $r_1(\mathbf{x})/k + c_{12}$ and $r_2(\mathbf{x})/k + c_{21}$ in Eq. 1a and 1b, respectively. Thus, the model makes no explicit assumption on the mode of interaction between the species with the exception that the impact of interspecific competition is assumed to be stronger than or equal to the impact of intraspecific competition for each species.

Model initial conditions and simulation

The model (Eq. 1) is solved using a finite element method employed by the PDE Toolbox in Matlab (The MathWorks Inc. 2020). In all model simulations, $R_\Omega = 10$ and the target edge length of the finite elements is set to 0.16. Numerical integration is stopped before the population reaches the boundary of the computational domain Ω. In this way, neither the non-flux boundary conditions ($\nabla B_1 \cdot \mathbf{n} = \nabla B_2 \cdot \mathbf{n} = 0$, where $\mathbf{n}$ denotes the outward normal on $\partial\Omega$) nor the shape (circle) of the boundary bear influence on the model solution.

The initial population is assumed to be confined to a subset $\Omega_0 = \{\mathbf{x} \in \Omega : \| \mathbf{x} \| < R_{\Omega_0}\}, R_{\Omega_0} < R_\Omega$ in the centre of the computational domain Ω. In this paper, we choose $R_{\Omega_0} = 2$. High initial population densities are represented by spatially homogeneous initial conditions in Ω_0, i.e. $B_1(\mathbf{x},0) \equiv k_1$, $B_2(\mathbf{x},0) \equiv k_2$ for $\mathbf{x} \in \Omega_0$ with $k_1 + k_2 \leq k$. The representation of very low initial population densities requires a different approach; at such densities, individuals are not necessarily spread uniformly in space. For example, inoculation of low densities of bacterial cells initially leads to the formation of small, spatially segregated microcolonies (Eigentler et al. 2022), and invasion of mammal species into previously unoccupied habitats typically originate from a small number of individuals (Middleton 1930, Campbell et al. 2012). To represent this initial clustering in the model, each species is initially confined to a number of small patches within Ω_0 in which their density is set to carrying capacity. Unless otherwise stated, the locations of these initial patches are chosen uniformly at random in Ω_0 with no overlap and their total number is denoted by $N \in \mathbb{N}$. For brevity, we refer to this type of initial condition as a patch initial condition throughout the manuscript. Computationally, the spatial mesh used to numerically solve the model imposes restrictions on the location and size of such patches. Therefore, we randomly choose the initial patch positions for each species from the set of mesh nodes in Ω_0 and set that species to carrying capacity at the nodes and to zero everywhere else. It is noted that depending on the spatial scale and precise application of the model, initial patches created by this method may be larger than the size of a single individual. In these cases, it is reasonable to assume that such patches can be identified with single individuals (or breeding pairs) that were initially able to reproduce without interaction with competitors.

Competitive outcome

For species B_1, we define the competitive outcome of multispecies range expansion to be a time-dependent function, $\overline{B_1}^{\Omega}(t)$, quantifying the relative abundance of species B_1 across the whole computational domain at time $t > 0$. This is given by

$$\overline{B_1}^{\Omega}(t) := \frac{\int_\Omega B_1(\mathbf{x},t)\,d\mathbf{x}}{\int_\Omega \left(B_1(\mathbf{x},t) + B_2(\mathbf{x},t)\right) d\mathbf{x}}.$$

We focus mainly on competitive outcome at the chosen endpoint $t = t_{\text{final}}$ of the model integration, but refer to the temporal dynamics of this quantity where appropriate. The chosen value of t_{final} (here $t_{\text{final}} = 5$) is sufficiently large to ensure the area covered by range expansion is significantly larger than the area of Ω_0 in which the initial population patches are placed, but sufficiently small so that the population does not reach the boundary of the computational domain Ω during the simulation. Note that competitive outcome for B_2, denoted by $\overline{B_2}^{\Omega}$, is given by $\overline{B_2}^{\Omega} = 1 - \overline{B_1}^{\Omega}$. Due to this simple relationship and for ease of exposition, throughout the paper we only refer to the competitive outcome for species B_1.

Area covered by range expansion

We further quantify the area covered by range expansion. Like competitive outcome, the area covered by range expansion, $A(t)$, is defined to be a time-dynamic quantity that measures the area in which the total population exceeds 10% of the carrying capacity at time $t > 0$. This is given by

$$A(t) = \text{Area}\left(\left\{\mathbf{x} \in \Omega : B_1(\mathbf{x},t) + B_2(\mathbf{x},t) > \frac{k}{10}\right\}\right),$$

where Area(·) denotes the area of a set in the Euclidean sense.

Front propagation metric

The relation between Euclidean distance and propagation time used in defining the access to free space score in homogeneous environments (Eigentler et al. 2022) does not hold in

spatially heterogeneous landscapes. Therefore, in this section, we define new tools to predict competitive outcome that take into account spatial heterogeneities in the landscape.

In order to make predictions regarding competitive outcome, we first determine the times that a population initially located in a small patch at $\mathbf{x} \in \Omega$ would take to propagate from $\mathbf{x}$ to some distant point $\mathbf{y}$ along each possible path in the absence of any competitive interaction. We then define the front propagation metric to be the shortest such time taken. This approach is motivated by earlier work on single-species range expansion which showed that a 'least-time principle' accurately predicts range expansion trajectories (Möbius et al. 2021). A rigorous definition is as follows. Denote the set of all paths from $\mathbf{x}$ to $\mathbf{y}$ by

$$\mathcal{P}(\mathbf{x},\mathbf{y}) := \{P = p([0,1]) \subset \Omega,$$

where $p:[0,1] \to \Omega : p$ is piecewise smooth, $p(0) = \mathbf{x}$, $p(1) = \mathbf{y}\}$. For a given path $P \in \mathcal{P}(\mathbf{x},\mathbf{y})$, the time taken to move along the path is given by

$$I(P) := \int_P \frac{1}{c(\mathbf{x})}\, ds = \int_0^1 \frac{1}{c(p(\tau))} \parallel p'(\tau) \parallel d\tau\,,$$

where $0 < c(\mathbf{x}) < \infty$ represents the propagation speed along the path P. The propagation speed $c(\mathbf{x})$ varies across the spatial domain due to the heterogeneous landscape. We define the front propagation metric from $\mathbf{x}$ to $\mathbf{y}$ as the shortest time to propagate from $\mathbf{x}$ to $\mathbf{y}$ along any path, i.e.

$$t_{\mathrm{FP}}(\mathbf{x},\mathbf{y}) := \inf_{P \in \mathcal{P}(\mathbf{x},\mathbf{y})} I(P)\,. \tag{2}$$

The infimum exists because $I(P) \geq 0$. We show in the supplement (Supporting information) that $t_{\mathrm{FP}}(\mathbf{x},\mathbf{y})$ is a metric in the mathematical sense.

Note that for our definition of the front propagation metric t_{FP} to hold, certain conditions are required on $c(\mathbf{x})$ to guarantee that the integral in Eq. 2 exists. Choosing $c(\mathbf{x})$ to be piecewise smooth would be sufficient and we believe this condition could be considerably relaxed. Moreover, we note that for computation of t_{FP}, spatial structure of the landscape is required to occur on the same (or coarser) scale than that of the domain discretisation to ensure accuracy. However, theoretically, the definition may fail on landscapes that have, for example, a full fractal structure to an infinitesimal level. In such cases, it is not clear whether the set $\mathcal{P}(\mathbf{x},\mathbf{y})$ includes the shortest path between $\mathbf{x}$ and $\mathbf{y}$. Hence and given that we are principally interested in the numerical implementation of the metric, we do not pursue a definitive set of necessary conditions on the propagation speed here.

It is well known that pulled travelling wave solutions (that is, wave fronts whose dynamics are governed only by their leading edges where linear terms dominate) exist for system Eq. 1 in spatially homogeneous domains. The minimum speed of these travelling waves is given by $c = 2\sqrt{rd}$. It can be shown that a large class of front solutions to system Eq. 1 asymptotically approach the dynamics of this minimum speed travelling wave (Stokes 1976). For spatially heterogeneous landscapes, we therefore reasonably assume the local front propagation speed to be $c(\mathbf{x}) = 2\sqrt{r(\mathbf{x})d(\mathbf{x})}$ for all $\mathbf{x} \in \Omega$. Numerical simulations confirm that this is indeed a reasonable approximation and is in agreement with earlier results (Korolev et al. 2012). Finally, we assume that both species undergo the same growth and diffusion dynamics in the absence of a competitor species (i.e. $r_1(\mathbf{x}) = r_2(\mathbf{x}) =: r(\mathbf{x})$ and $d_1(\mathbf{x}) = d_2(\mathbf{x}) =: d(\mathbf{x})$). In this case, the expansion fronts of both species are governed by the same expansion speed. We provide more information on relaxing this assumption in the Discussion section and the Supporting information.

Numerically, t_{FP} is computed by discretising the computational domain Ω into a weighted graph and applying Dijkstra's algorithm. Nodes of the graph are defined to be the centres of the finite elements of the domain discretisation. Graph edges connect graph nodes of elements that share edges of the finite elements. Graph edges are weighted by the time a front would require to travel along the edge, with its speed being approximated by the mean of the front speeds $c(\mathbf{x})$ evaluated at both nodes. In other words, a graph edge connecting graph nodes at positions $\mathbf{x}$ and $\mathbf{y}$ is assigned weight $\parallel \mathbf{x} - \mathbf{y} \parallel / (\sqrt{r_i(\mathbf{x})d_i(\mathbf{x})} + \sqrt{r_i(\mathbf{y})d_i(\mathbf{y})})$. Crucially, calculation of t_{FP} only requires as input the front propagation speed $c(\mathbf{x})$. Therefore, computational cost is independent of the complexity of the corresponding PDE system. Finally, we note that t_{FP} could alternatively be computed by numerically solving the Eikonal equation using the fast marching method (Möbius et al. 2021).

Voronoi tessellations

We now define a classification of the initial condition by performing a Voronoi tessellation with respect to the metric t_{FP}. That is, given $N \in \mathbb{N}$ initially occupied patches centred at $\mathbf{x}_1, \ldots \mathbf{x}_N \in \Omega_0$ we denote by $\Delta^{\Omega}_{B_1}$ and $\Delta^{\Omega}_{B_2}$ the sets that comprise points closest to initial patches of B_1 and initial patches of B_2, respectively. These sets are defined by

$$\Delta^{\Omega}_{B_i} := \left\{ \mathbf{x} \in \Omega : \min_{\mathrm{y_k} \in \mathcal{B}_i} t_{FP}(\mathbf{x}, \mathrm{y_k}) \leq \min_{\mathrm{y_l} \in \mathcal{B}_j} t_{FP}(\mathbf{x}, \mathrm{y_l}), i \neq j \right\},$$

where $\mathcal{B}_i := \left\{ \mathbf{x} \in \{\mathbf{x}_1, \ldots \mathbf{x}_N\} : B_i(\mathbf{x}, 0) > 0 \right\}, i = 1, 2$.

This Voronoi tessellation provides a classification for the whole computational domain ($\Delta^{\Omega}_{B_1} \cup \Delta^{\Omega}_{B_2} = \Omega$). Therefore, it cannot provide a prediction of range expansion properties for times before the population reaches the boundary of the domain. To account for the time dynamics, we modify the Voronoi tessellation by restricting it to sets providing an estimate for regions in Ω occupied by each species at any given time t (with the proviso that no competitive interactions take place). This is achieved by defining the Voronoi sets

$$\Delta_{B_i}(t) := \left\{ \mathbf{x} \in \Delta_{B_i}^{\Omega} : \min_{\mathbf{y} \in \mathcal{B}_i} t_{FP}(\mathbf{x}, \mathbf{y}) \leq t \right\}, \quad i = 1, 2.$$

The Euclidean area of these sets provides an upper bound for the area covered by each species in our model. Therefore, the Euclidean area of the union of Voronoi sets $\Delta_{B_1}(t) \cup \Delta_{B_2}(t)$ represents an estimate of the area covered by range expansion of the whole population at time t, as defined above.

Finally, we use these restricted sets to classify the initial condition for species B_i, $i=1, 2$, using a single number $V_i(t) \in [0,1]$, termed the Voronoi index $V_i(t)$. The index is defined to be the relative area of $\Delta B_i(t)$, i.e.

$$V_i(t) := \frac{\text{Area}\left(\Delta_{B_i}(t)\right)}{\text{Area}\left(\Delta_{B_1}(t)\right) + \text{Area}\left(\Delta_{B_2}(t)\right)}, \quad i = 1, 2.$$

where Area(·) denotes the total area of a set (or collection of sets) in the Euclidean sense.

Intraspecies connectedness

Lastly, we define the notion of intraspecies connectedness. Essentially, this captures the number of distinct sectors associated with each species that arise via the Voronoi tessellation detailed above. Denote the boundary of the union of Voronoi sets $\Delta_{B_1}(t) \cup \Delta_{B_2}(t)$ by $\Gamma(t)$. We then classify points on Γ based on which Voronoi set they belong, i.e. we define $\Gamma_{B_i}(t) := \{\mathbf{x} \in \Gamma : \mathbf{x} \in \Delta_{B_i}(t)\}, i = 1, 2$. Finally, the intraspecies connectedness, M, is defined to be half the number points in the intersection between $\Gamma_{B_1}(t)$ and $\Gamma_{B_2}(t)$, i.e. $M(t) = \#(\Gamma_{B_1}(t) \cap \Gamma_{B_2}(t))/2$. Note that the intersection between $\Gamma_{B_1}(t)$ and $\Gamma_{B_2}(t)$ either contains zero or an even number of points. The intersection is finite because the intersection between the Voronoi sets $\Delta_{B_1}(t)$ and $\Delta_{B_2}(t)$ is a union of one-dimensional curves along which points are equidistant from initial patches of B_1 and B_2. Evenness follows from the closed shape of Γ (Fig. 2).

Results

Range expansion in spatially heterogeneous domains

With the methods for model analysis in place, we can now determine the effect of spatial landscape heterogeneities. For simplicity, we randomly split the landscape Ω into two types of environment in each independent model realisation. One type represents favourable environmental conditions (large r_1, r_2, d_1, d_2) and the other signifies challenging environmental conditions (small r_1, r_2, d_1, d_2). We assume that the environment remains fixed over the duration of a model simulation. There exist many methods to split the domain into favourable and challenging regions. In this section, we present results for domains that are obtained by linking the parameter landscape to a random surface with monofractal structure (see Supporting information for details). However, we show in the supplement that results do not depend on this particular choice of heterogeneity by confirming that they hold for other forms of spatially heterogeneous landscapes (Supporting information). In all heterogeneous landscapes considered, the dominant scale (defined by the largest connected region of one environment type) is large compared to the width of the travelling front (i.e. the region in which $0 < B_1 + B_2 < k$). However, isolated smaller patches may exist (Fig. 3). The assumption that the propagation speed can be approximated by $c(\mathbf{x}) = 2\sqrt{r(\mathbf{x})d(\mathbf{x})}$ may not hold in such patches due to their size. However, we do not expect these errors to significantly affect overall predictions and results because small patches have been shown to have negligible long-term effects on the dynamics of range expansion (Möbius et al. 2021).

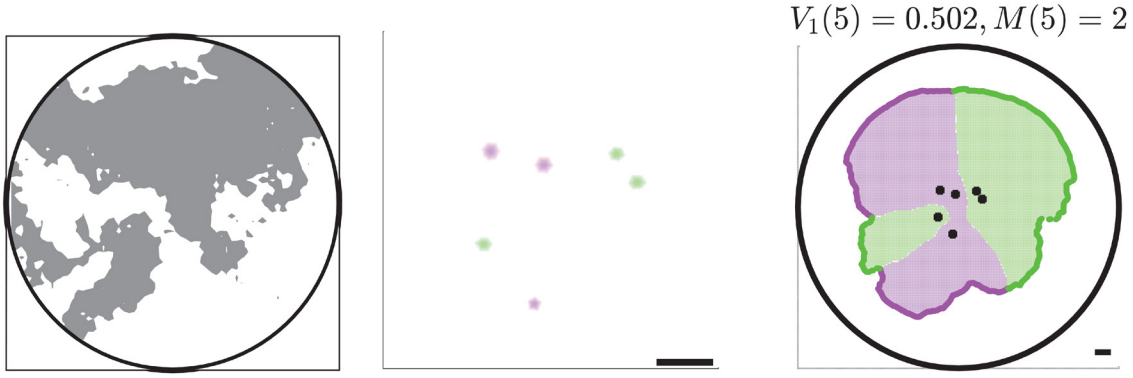

Figure 2. Voronoi tessellation with respect to front propagation metric. A Voronoi tessellation, i.e. the sets $\Delta_{B_1}(t_{\text{final}})$ (magenta) and $\Delta_{B_2}(t_{\text{final}})$ (green), where $t_{\text{final}}=5$, with respect to the front propagation metric t_{FP} is shown (right). The boundary of their union, used to calculate the intraspecies connectedness $M(t_{\text{final}})$ is highlighted. The initial cell patches are shown by black markers and are also visualised separately (middle). Note that the middle column shows a blow-up of the centre of the computational domain only. The scale bars are one unit length long. The underlying spatially heterogeneous domain is shown in the left column. Grey areas indicate good environmental conditions with $r=5$, $d=0.1$ and white areas indicate challenging environmental conditions with $r=2.5$, $d=0.05$.

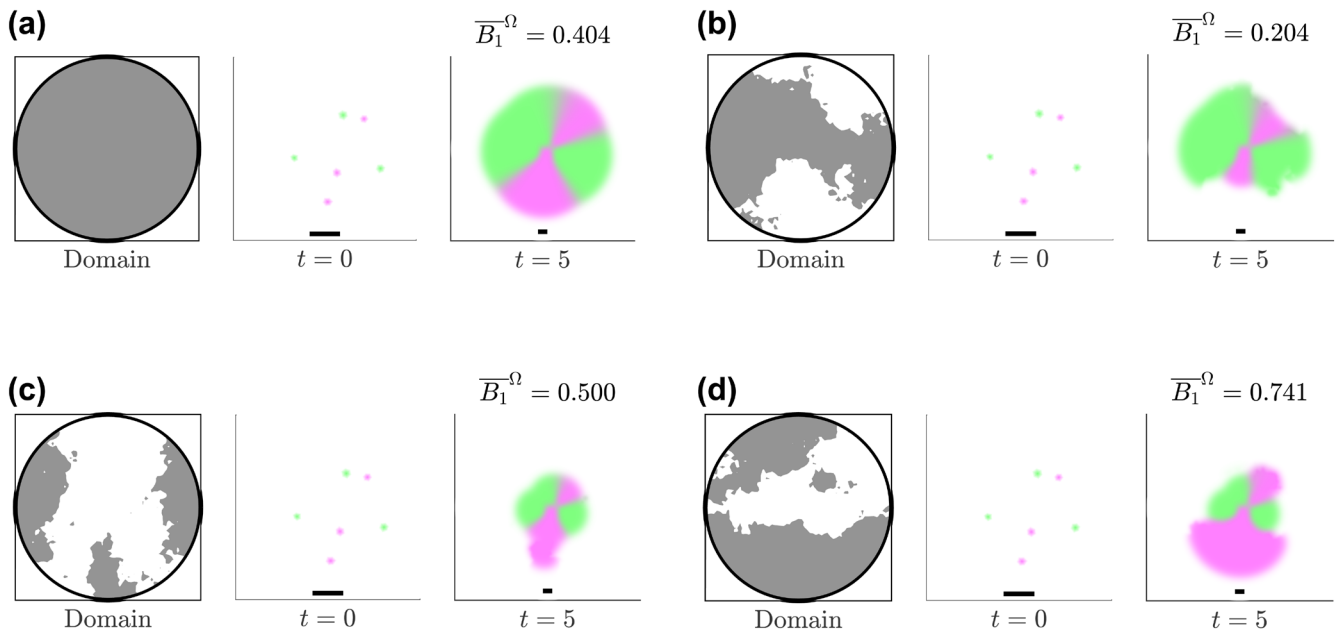

Figure 3. Spatial heterogeneities impact single model realisations. Four model realisations with identical initial conditions but different spatial domains are compared. (a) shows a model realisation on a spatially homogeneous domain, (b–d) on different spatially heterogeneous domains. For each triplet of plots, the left column shows the spatial structure of the domain. Good environmental conditions are shown in grey. The middle column shows the initial condition of the system in a blow-up of the centre of the spatial domain. The right column shows the model result at the defined endpoint. The scale bars are 1 unit length long. Species B_1 is displayed in magenta, species B_2 in green.

Competition for space

We start by restricting our focus on competition for space only. We do so by considering the dynamics of two differently labelled, but otherwise identical species B_1 and B_2. In terms of the model parameters, this scenario is achieved by setting $d_1 = d_2 =: d$, $r_1 = r_2 =: r$, $c_{12} = c_{21} = 0$. Unless otherwise stated, we use $k = 1$ throughout and $d = 0.1$, $r = 5$ to characterise favourable environments and $d = 0.05$, $r = 2.5$ to characterise challenging environments. Note that the parameters are chosen so that the width of the expansion front is small compared to the size of the region behind the front where the population is at carrying capacity. This is a realistic assumption in many contexts, for example the description of bacterial biofilms (Hallatschek et al. 2007), and modelling of plant ecosystems (Hoffmann et al. 2012, Yatat et al. 2018).

Landscape changes cause variability in competitive outcome and area covered by range expansion

We start by considering only changes in the parameter landscape across different model realisations. To cover a wide range of different parameter landscapes, we opt for a Monte Carlo approach in which 500 model realisations with independently chosen parameter landscapes (but fixed initial population distributions with a 1:1 ratio between both species) are performed for each of 18 chosen initial population densities covering three orders of magnitude in initial number of patches (from $N = 2$ to $N = 500$).

As highlighted by the example visualisations shown in Fig. 3 for $N = 6$, changes to the spatial landscape cause variability in competitive outcome and area covered by the range expansion. The same trends are observed for other initial population densities within our test range. Moreover, the range of competitive outcome decreases with increasing initial population density and the mean competitive outcome varies across initial population densities (Supporting information). We remark that this variability in competitive outcome highlights that the access to free space score used to predict competitive outcome in spatially homogeneous landscapes (Eigentler et al. 2022) is unsuitable as a predictor for the heterogeneous landscapes considered here. This is because the access to free space score depends only on spatial location of the initial population and thus would generate the same prediction for each model realisation. Success of the access to free space score predictions relies on constant propagation speeds throughout the domain, a property that does not hold in spatially heterogeneous landscapes. Hence, the alternative method detailed above is applied in this paper. As expected based on experimental literature (Gralka and Hallatschek 2019, Borer et al. 2020), our results show that, all else being fixed, spatial heterogeneities have a significant influence on range expansion in our theoretical framework.

Changes to initial population distribution cause variability only in competitive outcome

Next, we fix the parameter landscape and only change the initial population distribution across independent model realisations. Performing a Monte Carlo simulation in this setting reveals that changes in the initial population

distribution on a fixed landscape lead to variability in competitive outcome that decreases with increasing population density (Supporting information). However, no variability in the area covered by range expansion is observed (Supporting information). These results are in agreement with earlier work on a (fixed) spatially homogeneous environment on which the initial population distribution was varied (Eigentler et al. 2022).

Motivated by the results of this and the preceding section, we address in the remainder of this section how the two possible sources of variability (changes to initial population distribution and changes to spatial landscape) interact with each other. We investigate 1) whether one source of variability dominates; and 2) if predictions of competitive outcome and area covered can be made based on the landscape and initial population locations. Finally, in the following section we investigate 3) what the dominant mode of competition is if species interact antagonistically.

Variability in competitive outcome is a function of initial population density

We next extend our Monte Carlo approach by independently choosing at random both the parameter landscape and initial population distribution (keeping the initial species ratio fixed at 1:1) in each model realisation to assess how simultaneous changes of both properties affect range expansion. In model realisations representing high initial population densities, represented by spatially homogeneous initial conditions, only the parameter landscape is varied.

Simulations reveal that for each fixed initial population density, competitive outcome $\overline{B_i}^{\Omega}(t_{\text{final}})$ varies across independent model simulations. The observed mean $\mu(\overline{B_1}^{\Omega}(t_{\text{final}})) \approx 0.5$ for each initial population density and variability (i.e. standard deviation) in competitive outcome $\overline{B_i}^{\Omega}(t_{\text{final}})$ is maximal ($\sigma(\overline{B_1}^{\Omega}(t_{\text{final}})) \approx 0.15$) for $4 \leq N \leq 20$ and decreases with increasing initial population density for $N > 20$ ($\sigma((\overline{B_1}^{\Omega}(t_{\text{final}}))) \approx 0.065$ for $N=500$) (Fig. 4, Supporting information). For high initial population densities (represented by spatially homogeneous initial conditions), spatial homogeneity is preserved and a 1:1 initial ratio consistently leads to a competitive outcome $\overline{B_i}^{\Omega}(t_{\text{final}}) = 0.5$, despite the changing parameter landscape across different model realisations (Supporting information). [We also note a decrease in variability of competitive outcome if the number of initial patches is decreased to $N=2$ ($\sigma(\overline{B_1}^{\Omega}(t_{\text{final}})) \approx 0.116$). This also occurs in spatially homogeneous environments and we refer to (Eigentler et al. 2022) for an interpretation of this phenomenon.] The reported trends and the observed ranges of competitive outcome are very similar to those reported from spatially homogeneous domains (Eigentler et al. 2022), Supporting information). Therefore, we conclude that the initial population density remains the main determinant of variability, despite the landscape changes across different model realisations.

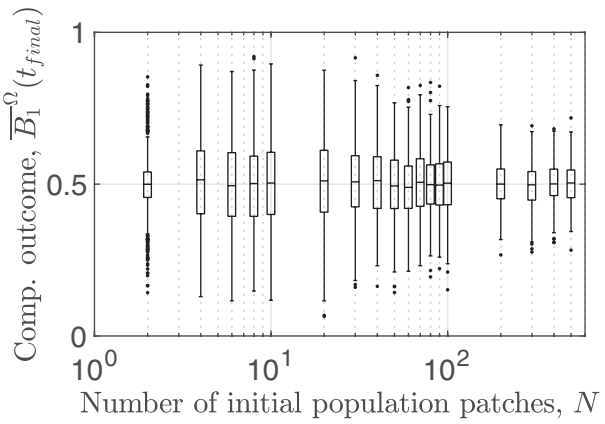

Figure 4. Variability in competitive outcome for identical species is a function of initial population density. The relation between initial population density and competitive outcome for the full dataset obtained through our Monte Carlo approach is shown. For results using different choices of spatially heterogeneous parameter landscapes see the Supporting information.

Variability in area covered by range expansion is determined by spatial heterogeneities

Analysis of data obtained through the Monte Carlo approach further reveals variability in the area covered by range expansion (Fig. 5, Supporting information). The extent of the variability is approximately identical across all initial population densities ($\sigma(A(t_{\text{final}}) \approx 42)$). Recall that such variability is not observed if the parameter landscape remains unchanged across different model realisations. Combined, we conclude that variability in the area covered by range expansion is independent of the initial population density. Instead, it is caused by changes in the spatially heterogeneous landscapes across different model realisations.

Finally we note that the area covered by range expansion is increasing and saturating with increasing initial population density, which leads to a decrease and saturation of relative standard deviation.

Voronoi tessellations predict range expansion, competitive outcome and spatial structure

We now detail how the Voronoi tessellations and the Voronoi index $V_i(t)$ determine a predictive relationship between the location of the initial patches and the resulting growth dynamics. Using the data from the Monte Carlo approach defined above, the following relationships were established.

First, the Voronoi tessellations provide accurate estimates of the area covered by the population during range expansion (Supporting information).

Second, the Voronoi index $V_i(t)$ and competitive outcome $\overline{B_i}^{\Omega}(t)$ are approximately linearly correlated for each initial population density. Thus, for fixed initial population density, the Voronoi index acts as an accurate predictor of competitive outcome (Fig. 6). The accuracy of these predictions is similar to that reported from the spatially homogeneous case for which an alternative prediction method was used (Eigentler et al. 2022). The predictive power of the Voronoi

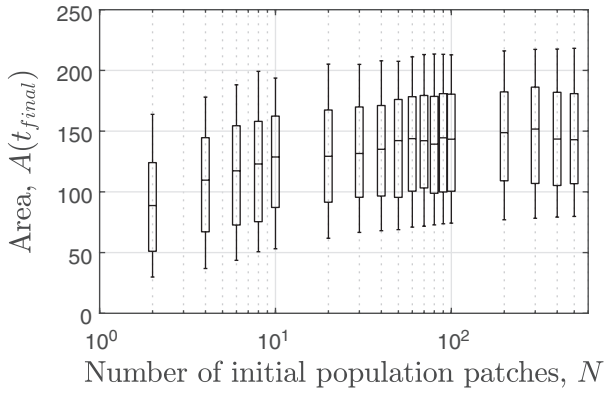

Figure 5. Landscape heterogeneity determines variability in area covered by range expansion. The relation between initial population density and area covered by range expansion is shown for the full dataset obtained through our Monte Carlo approach for identical species. For results using different choices of spatially heterogeneous parameter landscapes see the Supporting information.

index is time-invariant, even though both the Voronoi index $V_i(t)$ and the competitive outcome $\overline{B}_i^{\Omega}(t)$ are dynamic quantities that evolve over time during range expansion (Supporting information).

Third, the slope of the relation between the Voronoi index $V_i(t)$ and competitive outcome $\overline{B}_i^{\Omega}(t)$ is decreasing with increasing population density. The Voronoi tessellations accurately predict the spatial structure of the model solutions if the initial population density is low (Fig. 6b). This further translates to an approximate identity between the Voronoi index V_i and competitive outcome $\overline{B}_i^{\Omega}$ for low initial population densities (i.e. $V_i \approx \overline{B}_i^{\Omega}$). This occurs because species remain spatially segregated during range expansion and only colonise those areas closest to their initial patches. By contrast, the short distances between initial patches at high initial population densities lead to the development of more regions of overlap between the two species in the model solutions over time. These regions of overlap are not captured by the binary nature of the Voronoi tessellations (Fig. 6d, f) leading to deviations from the approximate identity between Voronoi index and competitive outcome. In these cases, changes in the initial patch configuration as measured by the Voronoi index have a smaller impact on competitive outcome (cf. Fig. 6a, c, e), which leads to the somewhat counter-intuitive conclusion that competition for space between the two species becomes stronger as the initial population becomes more scarce.

The results above were obtained for a range of fixed initial population densities, all of which were initiated with a 1:1 ratio between species (i.e. $\overline{B}_1^{\Omega}(0) = \overline{B}_2^{\Omega}(0) = 0.5$). However, the predictive power of the Voronoi index $V_i(t)$ is robust to variations in initial population ratio as is shown by additional model simulations with fixed initial population density and uniformly randomly chosen initial species ratio (i.e. $\overline{B}_1^{\Omega}(0) \sim \mathcal{U}(0,1)$) (Supporting information). While simulations show that increases in initial abundance of a species confers (on average) a competitive advantage, the Voronoi index $V_i(t)$ provides a more accurate prediction of competitive outcome $\overline{B}_i^{\Omega}(t_{\text{final}})$ than the initial abundance of the species $\overline{B}_i^{\Omega}(0)$ (cf. Supporting information).

Antagonistic interactions

We next consider species that interact antagonistically and investigate the relation between this interaction and spatial dynamics in range expansion. To this end, we set the coefficients in the killing terms to be positive, i.e. $c_{12} > 0$ and $c_{21} > 0$. We assume that species undergo the same growth dynamics in the absence of a competitor species (i.e. $d_1 = d_2$, $r_1 = r_2$, but see section 'Discussion' and Supporting information for a discussion on relaxation of this assumption) and set $c_{12} = 5c_{21}$ to create a strong asymmetry between the killing strengths. Note that in the absence of spatial dynamics, the model reduces to the competitive Lotka–Volterra equations. In the Lotka–Volterra model, stability of both single-species equilibria occurs, with the asymptotic solution behaviour depending on both model parameters and initial condition (bistability). For our parameter choice, convergence to the single-species equilibrium of B_2 occurs provided $B_1(0)/B_2(0) < 5$. Since we typically use a 1:1 initial ratio in our analysis, we refer to B_2 as the intrinsically stronger species throughout this section. Unless otherwise stated, we use the same growth and diffusion parameters as and set $c_{21} = 10$, $c_{12} = 50$ and $k = 1$. Note the order of magnitude difference between the killing coefficients and other model parameters. The large size of the killing coefficients ensures that coexistence (in a non-spatial sense) cannot occur as a long transient state.

Antagonistic interactions are the dominant mode of competition for high initial population densities only

We again perform Monte Carlo simulations with fixed initial species ratio, but randomly chosen locations of initial population patches, and randomly chosen landscapes. Resulting data show that for high initial population density (using both the patch initial conditions with large N (Fig. 7a, Supporting information) and spatially homogenous initial conditions (not shown)), competitive exclusion of the weaker species occurs consistently ($\overline{B}_1^{\Omega}(t_{\text{final}}) < 0.01$). By contrast, coexistence (through spatial segregation) is generally possible for lower initial population densities, but independent model realisations yield variable competitive outcomes with the extent of variability being similar to that observed for identical species ($\sigma(\overline{B}_1^{\Omega}(t_{\text{final}})) \approx 0.15$ for $2 < N < 20$; Fig. 7b–c, Supporting information). Further, similar to the case of identical species, variability in competitive outcome increases with decreasing initial population density (Fig. 7d, Supporting information). However, in contrast to the case of identical species, the mean competitive outcome $\overline{B}_1^{\Omega}$ decreases with increasing initial population density N. This shows that killing becomes the dominant mode of competition as the initial population density increases. It is important to note that a comparison with

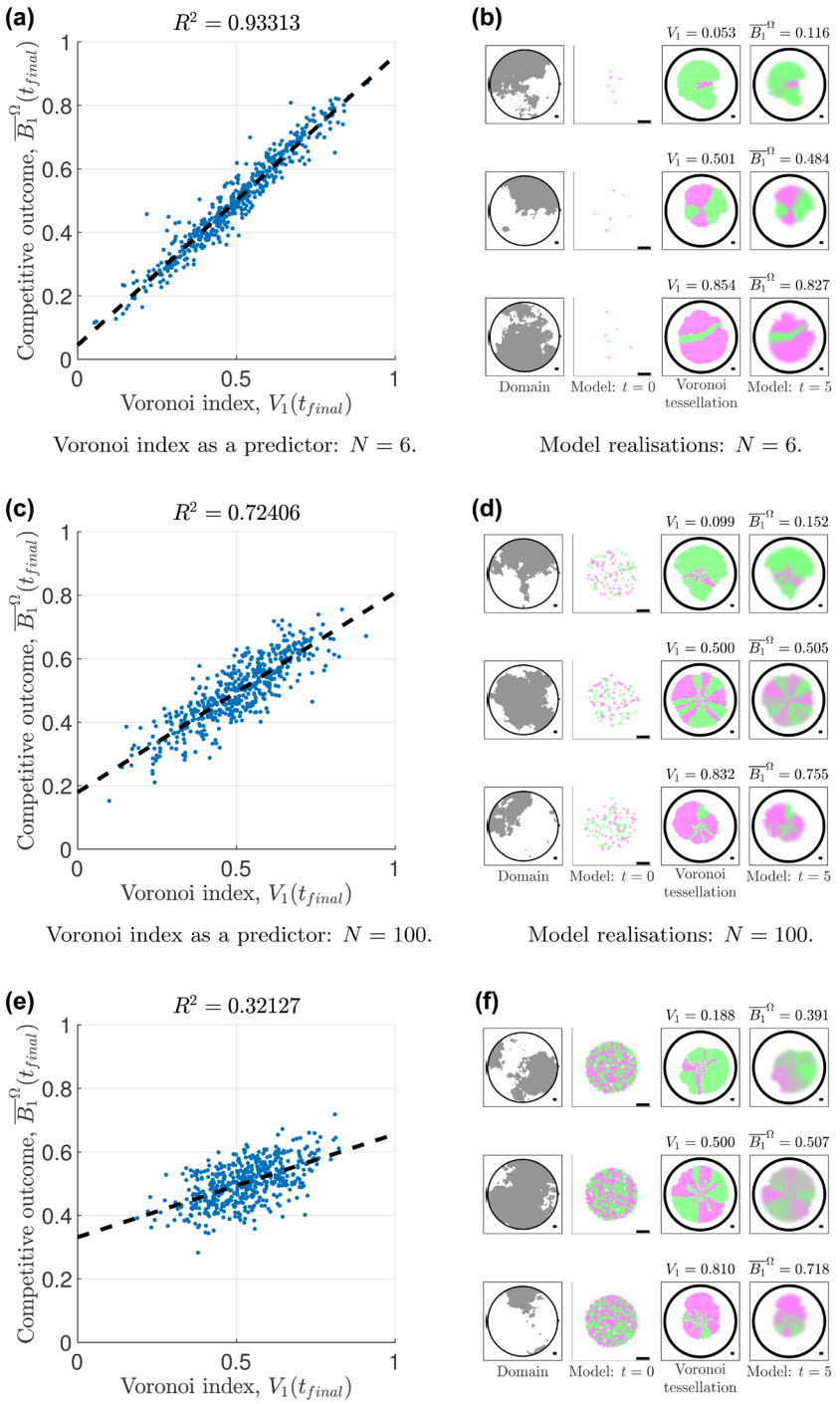

Figure 6. Voronoi tessellations predict competitive outcome. The relation between the Voronoi index V_1 and competitive outcome $\overline{B_1}^{\Omega}$ is visualised (blue dots) for three different initial population densities in (a, c, e). A line of best fit (black dashed) to the data is shown. For each initial population density, example model realisations are shown in (b, d, f). The first column in each of (b, d, f) shows the spatially heterogeneous domain; the second column shows the initial condition as a blow-up of Ω_0; the third column shows the prediction obtained by the Voronoi tessellation and the Voronoi index V_1; and the last column shows the densities at $t = t_{\text{final}}$, and the competitive outcome $\overline{B_1}^{\Omega}$. Species B_1 is displayed in magenta, species B_2 in green. Note that the boundaries between Voronoi sets in spatially homogeneous subsets of the spatial domain do not appear as perfect straight lines because the spatial discretisation of the domain in the calculation of the Voronoi sets. For results using different choices of spatially heterogeneous landscapes see the Supporting information.

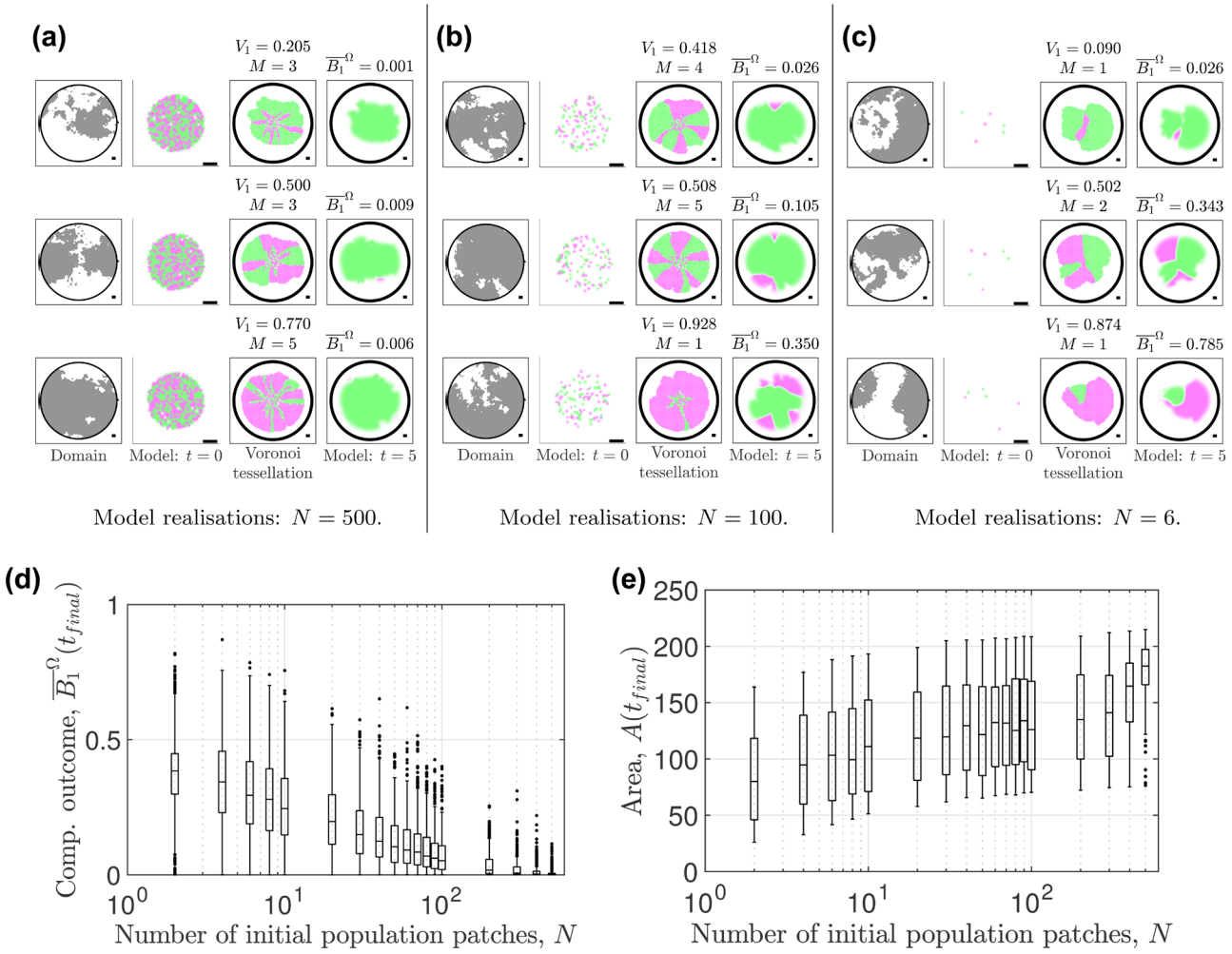

Figure 7. Model simulation data for two antagonistic species. Example model realisations are shown in (a–c) for a selected choice of initial population densities. The first column in each of (a–c) shows the spatially heterogeneous domain with grey areas indicating favourable environments; the second column shows the initial condition as a blow-up of Ω_0; the third column shows the prediction obtained by the Voronoi tessellation, the Voronoi index V_1 and the intraspecies connectedness M; and the last column shows the densities at $t = t_{\text{final}}$ and the competitive outcome $\overline{B_1}^{\Omega}$. Species B_1 is displayed in magenta, species B_2 in green. The relation between initial population density and competitive outcome $\overline{B_1}^{\Omega}$ is shown in (d). In (e), the relation between initial population density and area covered by range expansion is shown. For results using different choices of spatially heterogeneous landscapes see the Supporting information.

data from spatially homogeneous environments highlights that landscape changes across different model realisations do not increase the range of competitive outcomes observed (Eigentler et al. 2022, Supporting information).

Finally, similar to the case of identical species, variability in area covered by range expansion is high for all initial population densities ($\sigma(A(t_{\text{final}})) \approx 41$; Fig. 7e, Supporting information). Mean area covered increases slightly with increasing initial population density. Again, no variability occurs in spatially homogeneous landscapes (Eigentler et al. 2022) or if the heterogeneous landscape remains fixed across different model simulations (Supporting information). Thus, we conclude that variability in area covered by range expansion is determined by the landscape changes across different model realisations, even if species interact antagonistically.

Competition for space is the dominant competitive mode for low initial population densities

Similar to the case of identical species, Voronoi tessellations provide an accurate prediction of the area covered by the range expansion (Supporting information). Moreover, for each given initial population density, the Voronoi index V_1 is correlated with competitive outcome $\overline{B_1}^{\Omega}$ (Fig. 8). However, for fixed Voronoi index V_1, high initial population densities yield lower competitive outcomes than low initial population densities on average (cf. Fig. 8a, c). This is in agreement with

the dependence of the average competitive outcome on the initial population density shown in Fig. 7d. Combined, this highlights that competition for space takes over from antagonisms as the dominant competitive mode as the initial population density decreases.

Intraspecies connectedness refines predictions of competitive outcome

By definition, the Voronoi index V_i does not account for antagonistic interactions between two species. This leads to a slight decrease in accuracy of the predictions of competitive outcome compared with the case of identical species (cf. Fig. 6a, 8a). We therefore refine our prediction by taking into account the intraspecies connectedness, M, of the initial population . We hypothesise that the more the initial population is separated into connected regions, the less these populations interact during range expansion (essentially, the inter-species boundary is shorter). Indeed, our data show that for fixed Voronoi index V_1, high intraspecies connectedness (low M) is beneficial to the weaker species B_1 and leads to a higher

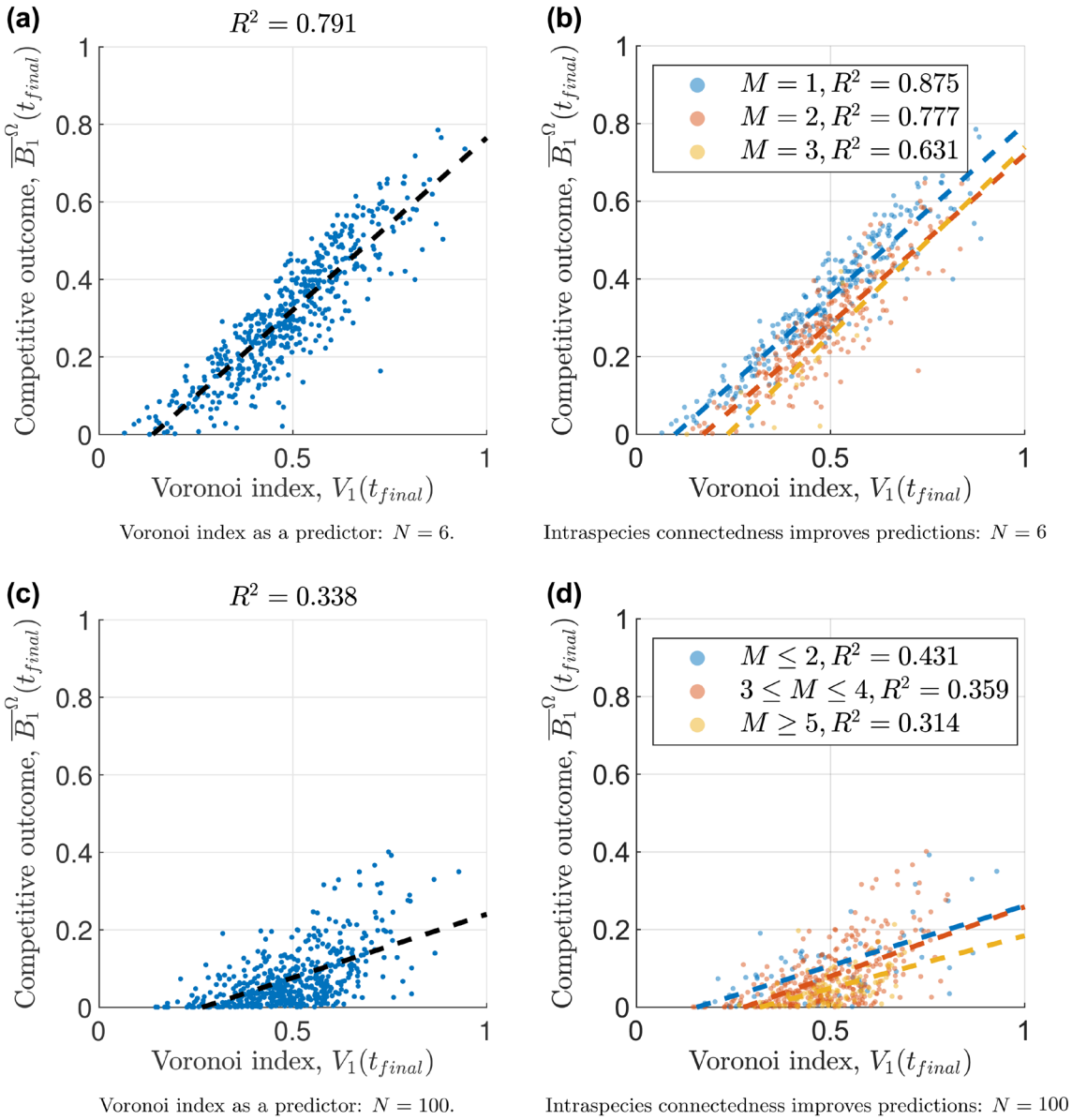

Voronoi index as a predictor: $N = 6$.

Intraspecies connectedness improves predictions: $N = 6$

Voronoi index as a predictor: $N = 100$.

Intraspecies connectedness improves predictions: $N = 100$

Figure 8. Voronoi tessellations and intraspecies connectedness predict competitive outcome for two antagonistic species. The relation between the Voronoi index V_1 and competitive outcome $\overline{B_1}^{\Omega}$ is visualised (blue circles) for two different initial population densities in (a, c). A line of best fit (black dashed) to the data is shown. In (b, d), the data shown in (a, c) is filtered by the intraspecies connectedness M. Dashed lines indicate lines of best fit to the filtered data. Note that there are 263, 218 and 17 data points for $M=1$, $M=2$ and $M=3$, respectively, in (b) and 65, 331 and 104 data points for $M \leq 2$, $3 \leq M \leq 4$ and $M \geq 5$, respectively, in (d). For results using different choices of spatially heterogeneous landscapes see the Supporting information.

competitive outcome $\overline{B_1}^{\Omega}$ and vice versa. We confirmed that application of the intraspecies connectedness M as a filter to the Voronoi index V_1 increases the accuracy of predictions of competitive outcome $\overline{B_1}^{\Omega}$ if the initial population density is low (Fig. 8b, d).

Discussion

Previous theoretical and experimental studies have uncovered a wide range of (potentially species-specific) mechanisms underpinning competition during multi-species range expansion (Burton et al. 2010, Richter et al. 2012, Weber et al. 2014, Goldschmidt et al. 2017, Aguilera et al. 2019, Legault et al. 2020). In this paper, we address the impact of spatial heterogeneities in environmental conditions on competition within multi-species range expansion. We reveal that 1) predictions of area covered and competitive outcome can be made using a Voronoi tessellation with respect to a suitable metric; 2) for high initial population densities, antagonisms are the dominant mode of competition during range expansion, while for low initial populations densities, the initial distribution determines competitive outcome; 3) the initial population density is the main determinant of variability in competitive outcome; and 4) landscape heterogeneities are the main cause of variability in the area covered by range expansion.

We highlight that during range expansion of identical (but differently labelled) species, the initial species distribution determines competitive outcome (Fig. 6). The importance of the initial species distribution has previously been highlighted in the context of microbial range expansion (van Gestel et al. 2014, Bronk et al. 2018, Goldschmidt et al. 2021, Eigentler et al. 2022) and occurs because the identical species engage in a 'race for space'. We utilise the importance of the spatial dynamics to show that spatial structure and global outcome can be predicted accurately by a Voronoi tessellation with respect to an appropriate metric (Fig. 6b, d, f) This predictor requires as input only information on the spatial structure of the environment, the response of each species to the environment and the initial species distribution. Crucially, no information about the interaction between the species is needed. Indeed, the assumption that descendants colonise areas closest to their ancestors has been experimentally verified (in spatially homogeneous environments only) using microbial species (Lloyd and Allen 2015, Chacón et al. 2018). While the assumption that competing species are identical is restricting in practice, it presents the ideal test case to reveal the impact of spatial dynamics on competition for related species and forms a basis for further investigation of multi-species range expansion in which other competitive interactions occur.

Our analysis reveals that during multi-species range expansion in which species interactions are subject to antagonistic actions, competition for space remains the dominant mode of competition for low initial population densities, even if the strength of antagonistic actions between species is strongly skewed (Fig. 8). This asymmetry prevents the Voronoi index and tessellations predicting spatial structure and competitive outcome with the same degree of accuracy as in the case of identical species (cf. Fig. 6b and 7c for example). However, accuracy can be improved by filtering data with respect to intraspecies connectedness – an estimate of the total length of species-to-species interface based on the initial conditions (Fig. 8b, d). The dominance of competition for space over antagonistic mechanisms for low initial population densities is in agreement with modelling studies and field observations that show that traits enhancing dispersal abilities are selected for within population fronts during range expansion (Travis and Dytham 2002, Phillips et al. 2008).

Our model analysis highlights that if species interact through antagonistic actions, species coexistence can occur through spatial segregation with limited overlap between the species along species-to-species interfaces. Therefore, spatial segregation offers protection from competitors. In particular, the majority of the population within the expansion front is unaffected by the antagonistic actions. This enables an intrinsically weaker species to coexist with a stronger competitor, provided the former is able to spatially segregate from its competitor in the early stages of range expansion. This highlights that classical mechanisms commonly associated with enabling coexistence, such as a tradeoff between local competitiveness and dispersal abilities (Levins and Culver 1971, Horn and MacArthur 1972, Hassell et al. 1994, Tilman 1994, Gravel et al. 2010) or non-transitive competitive hierarchies ('rock–paper–scissors') (Kerr et al. 2002, Reichenbach et al. 2007, Avelino et al. 2019, Lowery and Ursell 2019) are not necessarily required for coexistence to occur. Instead, our results show that spatial dynamics alone are sufficient to generate coexistence in range expansion originating from low initial population densities.

The model revealed that, on average, spatially heterogeneous landscapes do not affect competitive outcome. However, outcomes from single realisations can be affected greatly by domain heterogeneities (Fig. 3). Moreover, variability in the area covered by range expansion is induced by spatial heterogeneities, independent of the initial population density (Fig. 5, 7e). These results highlight the importance of considering landscape heterogeneities when implementing human-driven interventions in ecological systems. Our results predict that in cases where large numbers of organisms are introduced and undergo range expansion simultaneously (e.g. in the addition of biofertilizers to soil, Arroyave-Toro et al. 2017, Calvo-Garrido et al. 2019), spatial landscape heterogeneities would be rendered insignificant. By contrast, landscape heterogeneities and initial population distributions would need to be carefully considered in applications for which only a small number of individuals are added into a system (e.g. rewilding of mammals, Lorimer et al. 2015).

We focussed our analysis on a generic competition model in which dynamics of species in the absence of interspecific competition are governed by logistic growth and diffusion. However, we argue that our method could be extended to

species whose growth and dispersal behaviour is governed by other functional responses. Generalisation would only require the calculation/estimation of the front propagation speed $c(\mathbf{x})$ used in the definition of the front propagation metric t_{FP}. If front expansion dynamics cannot be approximated by pulled travelling waves, the front expansion speed $c(\mathbf{x})$ may additionally depend on other model parameters such as the population's carrying capacity or intraspecific competition coefficients (which may also be space-dependent). Therefore, calculation of an estimate of $c(\mathbf{x})$ may not be as straightforward as for the model considered in this paper, but could nevertheless be approximated by numerical or field experiments. Moreover, we note that estimation of $c(\mathbf{x})$ may fail on landscapes with heterogeneities on a small scale that keep propagation speeds in perpetual transients. Despite these caveats, it is important to note that given $c(\mathbf{x})$ can be estimated, the computational cost of the front propagation metric t_{FP} does not scale with the complexity of the system. This presents a clear advantage over the numerical integration of a PDE system, whose computational cost increases with system complexity (e.g. due to increased number of species, explicit description of resources, more complex functional responses in growth and flux terms). Moreover, our method could be generalised to two or more species whose growth and dispersal dynamics differ from each other. In such a case, the front expansion speed $c(\mathbf{x})$ would differ for each species and therefore would require the definition of separate metrics. However, even an increase in the number of species would not lead to a significant increase in computational cost of the predictive method. For a mathematically rigorous definition of the Voronoi sets and indices in this case, see the Supporting information.

We further note that we restricted our analysis to a finite time interval. Within this time interval, the dynamic predictions provided by the Voronoi tessellations were shown to be accurate for all times (Supporting information). We therefore hypothesise that the predictive power of the Voronoi tessellations would continue to hold for range expansion taking place over longer timescales, provided the computational domain is sufficiently enlarged. For antagonistic species, the stronger competitor continually invades regions occupied by the weaker species. However, simultaneous expansion of the weaker species' sectors along the edge of the population front creates a balance that enables coexistence (Fig. 7). We hypothesise that such a balance is stable over long times provided sectors of the inferior competitor are sufficiently large. Future work could rigorously establish conditions, such as a critical patch size, for such behaviour to occur.

Finally, we note that our framework assumes that expanding populations cannot invade existing, fully colonised patches. In mathematical terms, this is modelled by a density dependent diffusion term. This is a realistic assumption for many ecosystems (Korolev et al. 2012, Stefanic et al. 2015, Cozzi et al. 2018, Matoz-Fernandez et al. 2020), but presents a possible limitation of our approach. Through a comparison between results from Eq. 1 and a model with constant diffusion coefficients, we find that relaxing this assumption has only a limited impact on competitive outcome (Supporting information). For identical species, deviations in competitive outcome are minimal. For antagonistically interacting species, the weaker competitor is detrimentally affected by such a change in diffusion coefficient, but the magnitude of the impact is small. Thus, we conclude that the predictive power of our approach could be extended to ecosystems in which the assumption of limited dispersal into occupied regions does not hold.

Conclusion

From the human perspective, range expansion is becoming an increasingly important process across many different spatial and temporal scales. Its significance extends from applications of fungal species and genetically modified, biofilm-forming microbes in biological, medical and industrial settings (Dzianach et al. 2019, Martignoni et al. 2020) to conservation programs for plant and animal species whose habitats are shifting polewards (or towards higher altitudes) due to climate change (Rosenzweig et al. 2007). Our results reveal that traits required for competitive success during range expansion starkly differ from those characterising competitive fitness in equilibrium settings if range expansion originates from low population density. This shows that intrinsically weaker species are able to persist (or in rare cases even outcompete) stronger species during range expansion, provided they are able to perform well in the 'race for space' that determines competitive outcome. Thereby, our results provide a complement to field studies and evolutionary models that have shown dispersal traits within single species are selected for within the expansion front (Travis and Dytham 2002, Phillips et al. 2008). While our theoretical framework is deliberately kept simple so as to be applicable in a general setting, the model and methods form a foundation for extensions and applications to specific ecosystems. Adaptations of the framework to specific species in specific environments would require field data on an ecosystem-wide scale. Such data is becoming increasingly available thanks to advances in remote sensing technologies (Deblauwe et al. 2012) and machine learning applications (Lary et al. 2016) which highlights the potential of the theoretical framework to support future work.

Acknowledgements – We are grateful to members of the Stanley-Wall lab and Prof. Cait E. MacPhee (University of Edinburgh) for helpful discussions.
Funding – Work presented in this paper was funded by the Biotechnology and Biological Science Research Council (BBSRC) (BB/P001335/1, BB/R012415/1).

Author contributions

Lukas Eigentler: Conceptualization (lead); Data curation (lead); Formal analysis (lead); Methodology (lead); Project administration (equal); Software (lead); Validation (lead); Visualization (lead); Writing – original draft (lead). **Nicola R. Stanley-Wall**: Conceptualization (supporting); Funding acquisition (lead); Project administration (equal); Supervision (equal); Writing – review and editing (equal). **Fordyce A.**

Davidson: Conceptualization (supporting); Funding acquisition (equal); Methodology (supporting); Project administration (equal); Supervision (equal); Writing – original draft (supporting); Writing – review and editing (equal).

Data availability statement

Data are available from the Zenodo Repository <https://doi.org/10.5281/zenodo.6373699> (Eigentler 2022).

Supporting information

The Supporting information associated with this article is available with the online version.

References

Aguilera, M. A. et al. 2019. Asymmetric competitive effects during species range expansion: an experimental assessment of interaction strength between 'equivalent' grazer species in their range overlap. – J. Anim. Ecol. 88: 277–289.

Arroyave-Toro, J. J. et al. 2017. Biocontrol activity of *Bacillus subtilis* EA-CB0015 cells and lipopeptides against postharvest fungal pathogens. – Biol. Control 114: 195–200.

Artois, J. et al. 2018. Changing geographic patterns and risk factors for avian influenza A(H7N9) infections in humans, China. – Emerg. Infect. Dis. 24: 87–94.

Avelino, P. P. et al. 2019. Predominance of the weakest species in Lotka–Volterra and May–Leonard formulations of the rock–paper–scissors model. – Phys. Rev. E 100: 042209.

Borer, B. et al. 2020. Spatial organization in microbial range expansion emerges from trophic dependencies and successful lineages. – Commun. Biol. 3: 685.

Bronk, B. von et al. 2018. Locality of interactions in three-strain bacterial competition in *E. coli*. – Phys. Biol. 16: 016002.

Burton, O. J. et al. 2010. Trade-offs and the evolution of life-histories during range expansion. – Ecol. Lett. 13: 1210–1220.

Buttery, N. J. et al. 2012. Structured growth and genetic drift raise relatedness in the social amoeba *Dictyostelium discoideum*. – Biol. Lett. 8: 794–797.

Calvo-Garrido, C. et al. 2019. Microbial antagonism toward *botrytis* bunch rot of grapes in multiple field tests using one *bacillus ginsengihumi* strain and formulated biological control products. – Front. Plant Sci. 10: 105.

Campbell, R. et al. 2012. Distribution, population assessment and activities of beavers in Tayside. – Scottish Natural Heritage Commissioned Report No. 540.

Chacón, J. M. et al. 2018. The spatial and metabolic basis of colony size variation. – ISME J. 12: 669–680.

Chesson, P. 2000. Mechanisms of maintenance of species diversity. – Annu. Rev. Ecol. Syst. 31: 343–366.

Cozzi, G. et al. 2018. Socially informed dispersal in a territorial cooperative breeder. – J. Anim. Ecol. 87: 838–849.

Crone, E. E. et al. 2019. Faster movement in nonhabitat matrix promotes range shifts in heterogeneous landscapes. – Ecology 100: e02701.

Deblauwe, V. et al. 2012. Determinants and dynamics of banded vegetation pattern migration in arid climates. – Ecol. Monogr. 82: 3–21.

Diekmann, O. 1979. Run for your life. A note on the asymptotic speed of propagation of an epidemic. – J. Diff. Equat. 33: 58–73.

Dzianach, P. A. et al. 2019. Challenges of biofilm control and utilization: lessons from mathematical modelling. – J. R. Soc. Interface 16: 20190042.

Eigentler, L. 2022. Data from: A theoretical framework for multi-species range expansion in spatially heterogeneous landscapes. – Zenodo Digital Repository, <https://doi.org/10.5281/zenodo.6373699>.

Eigentler, L. et al. 2022. Founder cell configuration drives competitive outcome within colony biofilms. – ISME J., in press, doi: 10.1038/s41396-022-01198-8.

Fraser, E. J. et al. 2015. Range expansion of an invasive species through a heterogeneous landscape – the case of American mink in Scotland. – Divers. Distrib. 21: 888–900.

Ghosh, P. et al. 2015. Mechanically-driven phase separation in a growing bacterial colony. – Proc. Natl Acad. Sci. USA 112: E2166–E2173.

Goldschmidt, F. et al. 2017. Successive range expansion promotes diversity and accelerates evolution in spatially structured microbial populations. – ISME J. 11: 2112–2123.

Goldschmidt, F. et al. 2021. Causes and consequences of pattern diversification in a spatially self-organizing microbial community. – ISME J. 15: 2415–2426.

Gralka, M. and Hallatschek, O. 2019. Environmental heterogeneity can tip the population genetics of range expansions. – eLife 8: e02701.

Gravel, D. et al. 2010. Patch dynamics, persistence and species coexistence in metaecosystems. – Am. Nat. 176: 289–302.

Hallatschek, O. et al. 2007. Genetic drift at expanding frontiers promotes gene segregation. – Proc. Natl Acad. Sci. USA 104: 19926–19930.

Hassell, M. P. et al. 1994. Species coexistence and self-organizing spatial dynamics. – Nature 370: 290–292.

Hastings, A. et al. 2005. The spatial spread of invasions: new developments in theory and evidence. – Ecol. Lett. 8: 91–101.

Hill, J. et al. 2001. Impacts of landscape structure on butterfly range expansion. – Ecol. Lett. 4: 313–321.

Hodgson, J. A. et al. 2012. The speed of range shifts in fragmented landscapes. – PLoS One 7: e47141.

Hoffmann, W. A. et al. 2012. Ecological thresholds at the Savanna-forest boundary: how plant traits, resources and fire govern the distribution of tropical biomes. – Ecol. Lett. 15: 759–768.

Horn, H. S. and MacArthur, R. H. 1972. Competition among fugitive species in a harlequin environment. – Ecology 53: 749–752.

Kerr, B. et al. 2002. Local dispersal promotes biodiversity in a real-life game of rock–paper–scissors. – Nature 418: 171–174.

Kinezaki, N. et al. 2010. The effect of the spatial configuration of habitat fragmentation on invasive spread. – Theor. Popul. Biol. 78: 298–308.

Korolev, K. S. et al. 2012. Selective sweeps in growing microbial colonies. – Phys. Biol. 9: 026008.

Lary, D. J. et al. 2016. Machine learning in geosciences and remote sensing. – Geosci. Front. 7: 3–10.

Legault, G. et al. 2020. Interspecific competition slows range expansion and shapes range boundaries. – Proc. Natl Acad. Sci. USA 117: 26854–26860.

Levine, J. M. and HilleRisLambers, J. 2010. The maintenance of species diversity. – Nat. Educ. Knowl. 3: 59.

Levins, R. and Culver, D. 1971. Regional coexistence of species and competition between rare species. – Proc. Natl Acad. Sci. USA 68: 1246–1248.

Lloyd, D. P. and Allen, R. J. 2015. Competition for space during bacterial colonization of a surface. – J. R. Soc. Interface 12: 20150608.

Lorimer, J. et al. 2015. Rewilding: science, practice and politics. – Annu. Rev. Environ. Resour. 40: 39–62.
Lowery, N. V. and Ursell, T. 2019. Structured environments fundamentally alter dynamics and stability of ecological communities. – Proc. Natl Acad. Sci. USA 116: 379–388.
Möbius, W. et al. 2021. The collective effect of finite-sized in homogeneities on the spatial spread of populations in two dimensions. – J. R. Soc. Interface 18: 20210579.
MacDonald, J. S. and Lutscher, F. 2018. Individual behavior at habitat edges may help populations persist in moving habitats. – J. Math. Biol. 77: 2049–2077.
Martignoni, M. M. et al. 2020. Investigating the impact of the mycorrhizal inoculum on the resident fungal community and on plant growth. – Ecol. Model. 438: 109321.
Matoz-Fernandez, D. et al. 2020. Comment on 'Rivalry in *Bacillus subtilis* colonies: enemy or family?' – Soft Matter 16: 3344–3346.
McPeek, M. A. 2012. Intraspecific density dependence and a guild of consumers coexisting on one resource. – Ecology 93: 2728–2735.
Middleton, A. D. 1930. 38. The ecology of the American grey squirrel (*Sciurus carolinensis* Gmelin) in. the British Isles. – J. Zool. 100: 809–843.
Moreau, C. et al. 2011. Deep human genealogies reveal a selective advantage to be on an expanding wave front. – Science 334: 1148–1150.
Okubo, A. et al. 1989. On the spatial spread of the grey squirrel in Britain. – Proc. R. Soc. B 238: 113–125.
Pejchar, L. and Mooney, H. A. 2009. Invasive species, ecosystem services and human well-being. – Trends Ecol. Evol. 24: 497–504.
Phillips, B. L. et al. 2008. Reid's paradox revisited: the evolution of dispersal kernels during range expansion. – Am. Nat. 172: S34–S48.
Reichenbach, T. et al. 2007. Mobility promotes and jeopardizes biodiversity in rock–paper–scissors games. – Nature 448: 1046–1049.
Richter, O. et al. 2012. Modelling the effect of temperature on the range expansion of species by reaction–diffusion equations. – Math. Biosci. 235: 171–181.
Rosenzweig, C. et al. 2007. Assessment of observed changes and responses in natural and managed systems. – In: Parry, M. L. et al. (eds), Climate change 2007: impacts, adaptation and vulnerability. Contribution of working group II to the fourth assessment report of the intergovernmental panel on climate change. Cambridge Univ. Press, pp. 79–131.
Stefanic, P. et al. 2015. Kin discrimination between sympatric *Bacillus subtilis* isolates. – Proc. Natl Acad. Sci. USA 112: 14042–14047.
Stokes, A. 1976. On two types of moving front in quasilinear diffusion. – Math. Biosci. 31: 307–315.
Templeton, A. 2002. Out of Africa again and again. – Nature 416: 45–51.
The MathWorks Inc. 2020. Partial differential equation Toolbox™ user's guide.
Tilman, D. 1994. Competition and biodiversity in spatially structured habitats. – Ecology 75: 2–16.
Travis, J. and Dytham, C. 2002. Dispersal evolution during invasions. – Evol. Ecol. Res. 4: 1119–1129.
Urban, M. C. 2015. Accelerating extinction risk from climate change. – Science 348: 571–573.
Valladares, F. et al. 2015. Species coexistence in a changing world. – Front. Plant Sci. 6: 866.
van Gestel, J. et al. 2014. Density of founder cells affects spatial pattern formation and cooperation in *Bacillus subtilis* biofilms. – ISME J. 8: 2069–2079.
Vos, C. C. et al. 2008. Adapting landscapes to climate change: examples of climate-proof ecosystem networks and priority adaptation zones. – J. Appl. Ecol. 45: 1722–1731.
Weber, M. F. et al. 2014. Chemical warfare and survival strategies in bacterial range expansions. – J. R. Soc. Interface 11: 20140172.
Wegmann, D. et al. 2006. Molecular diversity after a range expansion in heterogeneous environments. – Genetics 174: 2009–2020.
Whittaker, R. H. et al. 1973. Niche, habitat and ecotope. – Am. Nat. 107: 321–338.
Wilson, R. J. et al. 2009. Modelling the effect of habitat fragmentation on range expansion in a butterfly. – Proc. R. Soc. B 276: 1421–1427.
With, K. A. 1997. The application of neutral landscape models in conservation biology. – Conserv. Biol. 11: 1069–1080.
With, K. A. 2002. The landscape ecology of invasive spread. – Conserv. Biol. 16: 1192–1203.
Yatat, V. D. et al. 2018. A tribute to the use of minimalistic spatially-implicit models of Savanna vegetation dynamics to address broad spatial scales in spite of scarce data. – Biomath 7: 1812167.